The physics of ocean wave evolution within tropical cyclones

Ali Tamizi[a], Jose-Henrique Alves[b] and Ian R. Young[a*]

[a]Department of Infrastructure Engineering, The University of Melbourne, Vic 3010, Australia.
[b]Weather Program Office, NOAA Research, Silver Spring, MD, USA

[*]Corresponding authors: Email: ian.young@unimelb.edu.au

Abstract

A series of numerical experiments with the WAVEWATCH III spectral wave model are used to investigate the physics of wave evolution in tropical cyclones. Buoy observations show that tropical cyclone wave spectra are directionally skewed with a continuum of energy between locally generated wind-sea and remotely generated waves. These systems are often separated by more than 90^0. The model spectra are consistent with the observed buoy data and are shown to be governed by nonlinear wave-wave interactions which result in a cascade of energy from the wind-sea to the remotely generated spectral peak. The peak waves act in a "parasitic" manner taking energy from the wind-sea to maintain their growth. The critical role of nonlinear processes explains why one-dimensional tropical cyclone spectra have characteristics very similar to fetch-limited waves, even though the generation system is far more complex. The results also provide strong validation of the critical role nonlinear interactions play in wind-wave evolution.

Early Online Release: This preliminary version has been accepted for publication in *Journal of the Physical Oceanography*, may be fully cited, and has been assigned DOI 10.1175/JPO-D-21-0005.1. The final typeset copyedited article will replace the EOR at the above DOI when it is published.

1. Introduction

In tropical and sub-tropical regions tropical cyclones represent the major extreme meteorological events, generating winds in excess of 40 ms^{-1} and significant wave heights above 10m. Such systems are characterised by a well-formed translating vortex wind field with a calm-eye and winds that spiral-in towards the centre of the storm. The strength of the winds, the rapidly changing direction and the translation of the system all pose particular challenges for our ability to understand the physics of wind-wave evolution in such systems and to develop appropriate tropical cyclone wave models. Despite the apparent complexity of the forcing wind field, observations of waves in tropical cyclones show that there are many similarities to waves generated in relatively simple cases with approximately constant uni-directional winds (Young, 1998, 2006; Hu and Chen, 2011; Collins et al., 2018; Tamizi and Young, 2020). As a result, a range of simple parametric models have shown surprising ability to be able to predict tropical cyclone generated waves. It has often been speculated (Young, 2006; Young, 2017, Collins et al., 2018; Tamizi and Young, 2020) that this is because nonlinear wave-wave interactions play a dominate role in defining the tropical cyclone directional wave spectrum and hence the significant wave height, as they do for more simple wave generation cases. Despite this speculation and the many observational studies of tropical cyclone wave spectra, no study has yet been able to demonstrate the role of nonlinear wave-wave interactions in tropical cyclones.

The present paper uses a state-of-the-art spectral wave model to investigate the source-term balance within the tropical cyclone wave field. The model is capable of modelling the tropical cyclone wind and wave fields at high resolution (2km) and

Accepted for publication in *Journal of Physical Oceanography*. DOI 10.1175/JPO-D-21-0005.1.

exploring the relative importance of the processes of: atmospheric input, white-cap dissipation, swell decay and nonlinear wave-wave interaction.

The arrangement of the paper is outlined below. Following this Introduction, Section 2 provides an overview of observations of the tropical cyclone wave field. Section 3 describes models which have been used to represent both the wind and wave fields within tropical cyclones. The WAVEWATCH III model (henceforth WW3) is used throughout the paper and the model physics and its setup for the present application are described in Section 4. The spatial distribution of the wave field, as predicted by the WW3 model is described in Section 5 and compared with observations. The energy balance within the directional wave spectrum is investigated for all regions of the tropical cyclone spatial wave field in Section 6 and the role of nonlinear wave-wave interactions is highlighted. Finally, a discussion and conclusions section is included at Section 7.

2. Observations of tropical cyclone wave fields

Waves within tropical cyclones have previously been observed using in-situ buoys, aircraft-borne synthetic aperture radars (SAR) and scanning radar altimeters (SRA) and satellite altimeters (ALT). In-situ buoy observations have included studies by Patterson (1974), Whalen and Ochi (1978), Black (1979), Ochi and Chiu (1982), Ochi (1993), Young (1998, 2006), Hu and Chen (2011), Collins et al. (2018) and Tamizi and Young (2020). SAR observations were reported by Elachi et al. (1977), King and Shemdin (1978), Gonzalez et al. (1978), McLeish and Ross (1983), Holt and Gonzalez (1986), Beal et al. (1986), Wright et al. (2001) and Black et al. (2007). Scanning Radar Altimeter (SRA) observations have been reported by Wright et al.

Accepted for publication in *Journal of Physical Oceanography*. DOI 10.1175/JPO-D-21-0005.1.

(2001), Walsh et al. (2002), Black et al. (2007), Hwang (2016), Hwang and Fan (2017), Hwang et al. (2017), Hwang and Walsh (2016, 2018a,b) and Walsh et al. (2021). In-situ buoys, SAR and SRA measure the directional wave spectrum. In contrast, satellite altimeters measure only the significant wave height but have the advantage of a much more extensive spatial distribution of observations. Such ALT measurements have been reported by Young and Burchell (1986), Young and Vinoth (2013) and Tamizi and Young (2020).

The collective dataset from these studies reveals a generally consistent picture of the tropical cyclone wave field and the directional spectrum. Whereas the wind field within tropical cyclones (TC) can be described by a relatively simple vortex model with added asymmetry (Tamizi et al., 2020), the wave field is more complex. Ahead of the TC centre, the wave field is characterised by a combination of remotely generated waves radiating out from the intense wind region to the right of the centre of the TC and locally generated wind-sea. The remotely generated waves were generated in the intense wind regions near the centre of the storm, but their energy has propagated (group velocity) faster than the forward speed of the storm and outrun the TC. The locally generated wind-sea is aligned with the local wind and often propagates at angles up to and exceeding 90^0 relative to the remotely generated waves. The remotely generated waves also have peak frequencies much lower than the locally generated wind-sea. The phase speed of these waves at the spectral peak often exceeds the local wind speed.

The maximum values of significant wave height (H_s) occur to the right of the centre of the TC (Note, throughout the paper it is assumed that northern hemisphere storms

Accepted for publication in *Journal of Physical Oceanography*. DOI 10.1175/JPO-D-21-0005.1.

are being considered). In comparison to the wind field, the waves are more strongly right-left asymmetric. In the intense wind/wave region to the right of the TC centre, the wind and wave directions are more closely aligned. In the left rear quadrant of the storm, the waves become quite confused with the low frequency remotely generated waves often at angles between 120^0 and 180^0 compared to the wind direction (and wind-sea).

Tamizi and Young (2020) compiled an extensive dataset from National Data Buoy Centre (NDBC) (Evans et al., 2003) buoys, which consists of a total of 2,902 buoy records recorded during 353 individual TCs (hurricanes). This very extensive in-situ dataset is consistent with previous buoy observations and summarises the present observational understanding from this source. Tamizi and Young (2020) combined the data from multiple TCs by adopting a frame of reference moving with the TC, as previously used by Young (1998, 2006), Hu and Chen (2011) and Collins et al. (2018). Figure 1 shows the spatial distribution of the directional wave spectrum from the Tamizi and Young (2020) data. The figure shows the mean wind direction, the peak wave direction, together with the one-dimensional spectrum, $E(f)$ and the directional spreading function, $D(f,\theta)$. The direction spectrum, $E(f,\theta)=E(f)D(f,\theta)$ where $\int D(f,\theta)df=1$. For presentation purposes, both the one-dimensional spectra and the values of $D(f,\theta)$ shown in Figure 1 have been normalized, such that the maximum values are one (for $D(f,\theta)$, the maximum value at each frequency is one).

The mean wind direction and peak wave direction vectors in Figure 1 show the spatial distributions of wave direction propagation described above. As previously reported

Accepted for publication in *Journal of Physical Oceanography*. DOI 10.1175/JPO-D-21-0005.1.

by Young (1998, 2006), Hu and Chen (2011) and Collins et al. (2018), despite the fact that the spectrum consists of a combination of remotely generated waves and local wind-sea, the one-dimensional spectrum is generally unimodal with a high frequency face proportional to approximately f^{-4}. In the left rear quadrant of the TC, where the wind and wave directions differ by more than 90^0, there is some suggestion of bimodal behaviour, with a small high frequency peak in the one-dimensional spectrum.

As also shown by Young (2006), despite the fact that the high frequency wind-sea and remotely generated low frequency waves can be separated by more than 90^0, the directional spectrum is also generally not bi-modal. Rather, the directional spectrum is directionally skewed but there is a continuum of energy from high frequency to low frequency. As noted by Tamizi and Young (2020), the generation sources for both the low frequency remotely generated waves (intense winds to the right of the TC centre at an earlier time) and the high frequency wind-sea (local wind) are clear. However, as the low frequency remotely generated waves are often propagating faster than the local wind, it is reasonable to assume there is no wind input to the spectrum for these and slightly higher frequencies. The question then arises as to how the wave energy in the transition region between the wind-sea and the low frequency peak was generated and maintained?

As noted above, Wright et al. (2001), Walsh et al. (2002), Black et al. (2007), Hwang (2016), Hwang and Fan (2017), Hwang et al. (2017), Hwang and Walsh (2016, 2018a,b) and Wash et al. (2021) reported SRA data taken from aircraft flights through a number of hurricanes. The vast majority of the results are associated with

Accepted for publication in *Journal of Physical Oceanography*. DOI 10.1175/JPO-D-21-0005.1.

observations from two hurricanes, Bella (1998) and Ivan (2004). Walsh et al. (2021) report data from the more recent hurricane Lorenzo (2019). SRA spectra reported for the regions ahead of and left of the storm centre are very similar to the buoy data shown in Figure 1. They show a dominant remotely generated peak radiating out from regions near the intense wind crescent of the translating tropical cyclone wind vortex with a skewed high frequency wind-sea. Generally, these spectra are unimodal, as for the buoy data.

To the right of the storm centre the SRA spectra are very broad and possibly show tri-modal forms in the right rear quadrant, becoming bi-modal in the right front quadrant (see Black et al., 2007, their Figure 10). The tri-modal spectra in the right rear quadrant show one swell peak propagating towards the centre of the tropical cyclone, apparently generated somewhere to the south-east of the storm centre (assuming the TC is propagating towards the north). Such a propagation direction is difficult to explain, as a typical vortex wind field cannot explain the existence of such a wave generation source, so far from the storm centre. It is possible that this swell system is generated by some meteorological system separate from the tropical cyclone, although this seems unlikely, as the reported SRA data from both Bonnie and Ivan show this feature. Another possibility is that the directional ambiguity in the SRA was not resolved correctly, in which case, this peak would be “folded back” 180^0, appearing closer to one of the other swell peaks, making the spectra bi-modal.

The existence of bi-modal spectra is easily explained, as the combination of local wind-sea and swell generated at an earlier time in the intense wind regions of the translating tropical cyclone. However, tri-modal systems, with peaks at similar

Accepted for publication in *Journal of Physical Oceanography*. DOI 10.1175/JPO-D-21-0005.1.

wavenumbers (frequencies), do not seem consistent with a wind field of this nature. For a continuous wind field represented by a vortex and a storm propagating at a constant velocity of forward movement, swell should be continuously generated as the storm translates. How such a system would generate multiple, separated swell peaks is not obvious.

Although the buoy results shown in Figure 1 present a consistent description of the spatial distribution of the TC directional spectrum, wave buoys have only limited directional resolving ability (they measure only three components) (Young, 1994; Tamizi and Young, 2020). These limitations mean that the resulting spectra tend to be smoother and directionally broader than recorded by instruments with more active sensors (e.g. spatial wave gauge arrays) (Young, 1994). Hence, it is possible that some of the smooth transition in direction as a function of frequency may be an artifact of the limited directional resolving power of the buoys. If this is the case, then it may explain some of the differences with the SRA data. Unfortunately, the SRA publications mentioned above do not present comparisons with buoy overflights. However, as noted above, for most regions of the tropical cyclone wave field, the SRA spectra are generally consistent with buoy data. Resolving whether the differences are a limitation of the buoys, the SRA, the selected hurricanes, or all of these is beyond the scope of this paper and a subject for future research.

Accepted for publication in *Journal of Physical Oceanography*. DOI 10.1175/JPO-D-21-0005.1.

3. Models of tropical cyclone wind and wave fields

Wind Field Models

As noted above, it is common to approximate the tropical cyclone wind field using a simple vortex model (Holland, 1980, Willoughby et al., 2006; Holland et al. 2010). Holland (1980) represented the radial pressure profile within a TC as:

$$p = p_0 + \Delta p e^{-(R_m/r)^b} \tag{1}$$

where Δp is the central pressure drop, R_m is the radius to maximum winds, r is the radial distance from the centre of the TC and p_0 is the central pressure in the TC. Using this pressure profile, Holland et al. (2010) represented the surface (10m elevation) wind speed as

$$U_{10} = \left[\frac{100 b_s \Delta p \left(R_m / r \right)^{b_s}}{\rho e^{\left(R_m / r \right)^{b_s}}} \right]^x \tag{2}$$

ρ is the density of air and surface values are defined by the subscript s. Holland et al. (2010), approximated the exponent b_s by:

$$b_s = -4.4 \times 10^{-5} \Delta p^2 + 0.01 \Delta p + 0.03 \frac{\partial p}{\partial t} - 0.014 \phi + 0.15 V_{fm}^{x_a} + 1.0 \tag{3}$$

In (3), V_{fm} is the velocity of forward movement of the TC in units of [ms^{-1}], ϕ is the absolute value of the latitude in units of [deg], t is time, $\frac{\partial p}{\partial t}$ has units of [HPa hr^{-1}] and Δp has units of [HPa]. The exponent x in (2) can be expressed as

$$x = \begin{cases} 0.5 & \text{for } r \le R_m \\ 0.5 + (r - R_m) \dfrac{x_n - 0.5}{r_n - R_m} & \text{for } r > R_m \end{cases} \tag{4}$$

The exponent x_a in (3) is given by $x_a = 0.6(1 - \Delta p / 215)$. Following Holland et al. (2010), $x = x(r)$ and $x_n = x(r_n)$. The value x_n can be determined from (2) if measurements of the surface wind are available at a radius r_n from the TC centre.

Accepted for publication in *Journal of Physical Oceanography*. DOI 10.1175/JPO-D-21-0005.1.

The wind field defined by (2) to (4) is symmetric. Based on extensive scatterometer measurements in TCs, Tamizi et al. (2020) found that the asymmetry of the wind field can be approximated to first order by the vector addition of the velocity of forward movement to the wind field vectors. This approximation agrees with the findings of Holland (2008), Klotz and Jiang (2016, 2017) and Olfateh et al. (2017). Consistent with the results of Powell (1982) and Zhang and Uhlhorn (2012), Tamizi et al. (2020) found that the observed inflow angle is a function of both p_0 and V_{fm} with the maximum values occurring in the right rear quadrant ($\sim 35^0$) and the minimum values in the left front quadrant ($\sim 10^0$).

Wave Field Models

The fact that one-dimensional wave spectra within TCs are unimodal leads to the obvious comparison with fetch-limited spectra. Young (1998, 2006), Hu and Chen (2011), Collins et al. (2018) and Tamizi and Young (2020) have all considered the detailed spectral shape of the one-dimensional spectrum under TC conditions. Despite the complex wind conditions described above [(1) to (4)], these studies show that TC wave spectra are remarkably similar to fetch-limited spectra measured during approximately constant uni-directional winds. In particular, the fetch-limited scaling between non-dimensional energy and non-dimensional peak frequency, proposed by Hasselmann et al. (1973) (JONSWAP) and Donelan et al. (1985) holds

$$\varepsilon = a\nu^m \tag{5}$$

where $\varepsilon = g^2 E_{tot} / U_{10}^4$ is the non-dimensional energy and $\nu = f_p U_{10} / g$ is the non-dimensional peak frequency. The total energy is represented by $E_{tot} = \int E(f) df$, f_p

Accepted for publication in *Journal of Physical Oceanography*. DOI 10.1175/JPO-D-21-0005.1.

is the spectral peak frequency and g is gravitational acceleration. The coefficients a and m are typically determined from recorded data.

This same scaling has also been confirmed from airborne SRA data (Hwang 2016; Hwang and Fan 2017; Hwang et al. 2017; Hwang and Walsh 2016, 2018a,b).

Noting this "JONSWAP-type" scaling, several authors have developed relationships to determine the significant wave height in TCs based on JONSWAP fetch-limited relationships. Young and Burchell (1986), Young (1988a) and Young and Vinoth (2013) use the concept of an "extended fetch" where waves move forward with the TC to define an "equivalent fetch", which is a function of the velocity of forward movement, V_{fm} and the maximum wind velocity in the storm, V_{max}. The equivalent fetch is used to define the maximum significant wave height in the TC. Values at other locations in the storm are then related to this maximum value. Hwang (2016) and Hwang and Walsh (2016) use a "circular race track" model in which a fetch is defined as a function of the distance from the centre of the TC. The significant wave height is then determined at that point from a JONSWAP-type relationship (Hasselmann et al., 1973). These models are described in detail and reviewed in Young (2017).

Our understanding of the physics of fetch-limited growth is that there is an active balance between three physical processes: atmospheric input, S_{in}; white-cap dissipation, S_{ds} and nonlinear wave-wave interactions, S_{nl} (Hasselmann et al., 1973). The balance between these processes results in the observed spectral form and the scaling represented by (5). In the case of TC wave generation, Figure 1 shows that the

Accepted for publication in *Journal of Physical Oceanography*. DOI 10.1175/JPO-D-21-0005.1.

spectra are a combination of remotely generated waves (at the spectral peak) and locally generated wind-sea. As the spectral peak waves are generally propagating faster than the local wind, they receive no positive input from the wind. Hence, it is reasonable to assume that the spectral balance near the peak of the spectrum is very different to fetch-limited cases (i.e. $S_{in} \approx 0$ or negative). Despite this, the JONSWAP-type scaling represented by (5) holds, even when the peak frequencies in this relationship are apparently disconnected from the local wind. Further, even though the directional spectra in TCs are directionally skewed, the one-dimensional spectra are very similar to fetch-limited cases. Note, however, that the peak frequencies in TC cases are at much lower values of f_p and the wave ages of these peak waves, $U_{10} / C_p < 1$ (Tamizi and Young, 2020), where C_p is the phase speed of waves at the spectral peak.

The aim of this paper is to investigate the spectral balance under the complex forcing of a TC and understand the physical processes responsible for the observed spectra. To date, there has been speculation on the possible energy balance (i.e. S_{nl} dominates, Tamizi and Young, 2020) but no detailed evaluation.

4. Translating grid WW3 model

The WW3 model (Tolman, 1991, 2002; WW3DG, 2019) is widely used as a state-of-the-art operational and research wave model. The model has been validated in TC conditions by Moon et al. (2003), Tolman and Alves (2005) and Liu et al. (2017). One of the challenges in modelling TC waves is to have a grid of sufficient spatial extent to model the translation of the storm, whilst having a grid resolution which is sufficiently small to define the intense wind vortex near the eye of the storm, where

Accepted for publication in *Journal of Physical Oceanography*. DOI 10.1175/JPO-D-21-0005.1.

much of the important wave generation occurs. These requirements (fine grid of large spatial extent) pose computation limitations. To overcome these challenges, Tolman and Alves (2005) developed a moving grid version of WW3, where the computational grid can move forward with the TC. Following Tolman and Alves (2005) the deep water governing radiative energy balance equation relative to this moving grid system becomes

$$\frac{\partial E(f,\theta)}{\partial t}+\left(\overrightarrow{C_g}-\overrightarrow{V_{fm}}\right)\bullet\nabla_x E(f,\theta)=S(f,\theta) \tag{6}$$

where C_g is the group velocity of the spectral component, V_{fm} is the velocity of forward movement of the TC (the velocity of translation of the computational grid) and ∇_x is the spatial gradient differential operator. As noted above, the source term, S represents the physical processes active in wind-wave evolution. A number of source term (ST) packages have been proposed for WW3, including: ST3 (Janssen, 1991, 2004; Bidlot et al., 2007; Bidlot, 2012), ST4 (Ardhuin et al., 2010; Leckler et al., 2013) and ST6 (Donelan et al., 2006; Babanin et al., 2007; Babanin, 2011; Rogers et al., 2012; Zieger et al., 2015). Liu et al. (2017) have compared these source term packages in the context of TC wave prediction and determined that they produce similar results. Hence, we have opted for ST4, as it is the default package in WW3 and has an extensive user history.

A potential limitation in this (or any other) source term package is the representation of the nonlinear term, S_{nl}. All of these source term packages use the Discrete Interaction Approximation (DIA) (Hasselmann et al., 1985) to represent S_{nl}. This simplification is used because a full solution to the nonlinear term is computationally too expensive for two-dimensional spatial domains. The limitations of the DIA are

Accepted for publication in *Journal of Physical Oceanography*. DOI 10.1175/JPO-D-21-0005.1.

well documented (Cavaleri et al., 2007; Resio and Perrie, 2008; Perrie et al., 2013; Tolman, 2013; Rogers and Van Vledder, 2013). As noted by Liu et al. (2017) a simple substitution of the full solution for S_{nl}, although computationally expensive, may be possible for a limited range of computations. However, as each of the ST packages has been calibrated using the DIA, such a substitution would generally not produce acceptable results. A full recalibration of the WW3 model would be required. Therefore, the only practical option is to use the DIA, but to note the limitations that this brings.

Our simulations used the moving grid feature in WW3 and a computational grid of spatial extent 2000km x 1900km with a spatial resolution of $\Delta x = 2$km. The directional wave spectrum, $E(f,\theta)$ was defined with a directional resolution of $\Delta\theta =$ 5^0 (i.e. 72 direction band) and 50 frequency bands, defined by $f_n = 1.1 f_{n-1}$ with the first band $f_1 = 0.04$Hz and the last band $f_{50} =$ 4.27Hz.

The wind field used to drive the translating WW3 model grid consisted of the Holland vortex defined by (2) to (4) with first-order asymmetry provided by the vector addition of the velocity of forward movement, V_{fm} to the wind field vectors and an assumed constant inflow angle of 20^0 (Tamizi et al., 2020). The wind field model is then fully specified for given values of: Δp, V_{fm} and two spatial scale parameters, R_m - radius to maximum winds and R_{34} - the radius to gales, where the wind speed is equal to 34 knots (17.5ms^{-1}). For the results presented here, we consider a moderately intense TC with $\Delta p = 50$HPa, $R_m = 30$km, $R_{34} = 300$km and two cases of velocity of

Accepted for publication in *Journal of Physical Oceanography*. DOI 10.1175/JPO-D-21-0005.1.

forward movement, $V_{fm} = 2.5\text{ms}^{-1}$ and 5.0ms^{-1}. These values are typical for mature TCs (Tamizi et al., 2020).

5. Spatial distribution of wave spectra

Figure 2 shows contour plots of the spatial distribution of H_s for the two cases described above, as predicted by the WW3 model. The peak wave directions (arrows) are also shown. Note that for all plots, the TC is assumed to be propagating to the north (up the page) and is located at co-ordinates (0,0). The wave field shows the characteristic crescent shaped distribution with the largest waves to the right of the TC centre (Bretschneider, 1972; Patterson, 1974; Ross, 1976; US Army Corps of Eng., 1977; Whalen and Ochi, 1978; Black, 1979; Young and Burchell, 1986; Young, 1988a, 1988b, 2006; Young and Vinoth, 2013, Liu et al., 2017, Tamizi and Young, 2020). As shown in Figure 1, the wind direction (spiralling in towards the TC centre with an inflow angle of 20^0) and the peak wave direction are quite different. As is clear in Figure 2 and also shown from the buoy data of Figure 1, the peak waves radiate out from the intense wind regions near the TC centre. The largest waves to the right of the TC centre increase with increasing V_{fm}, consistent with the concept of an extended fetch to the right of the TC centre (Young, 1988a; Young and Burchell, 1986 and Young and Vinoth, 2013). However, ahead of the TC, values of H_s decay more rapidly for the faster moving storm. This is consistent with the wave field being dominated by remotely generated waves. For the slower storm, these waves can more easily outrun the storm and hence appear at large distances ahead of the TC centre.

Figure 3 shows the non-dimensional energy, ε as a function of non-dimensional frequency, ν. Figure 3a shows the buoy data of Tamizi and Young (2020) and Figure

Accepted for publication in *Journal of Physical Oceanography*. DOI 10.1175/JPO-D-21-0005.1.

3b shows the data for all grid points for the WW3 model case with $V_{fm} = 2.5$ms^{-1}. Note that points in the eye of the TC, where $U_{10} \approx 0$ms^{-1} have been excluded from the plot. Also shown on the figures are the fetch-limited result of Donelan et al. (1985), $\varepsilon = 6.36\times10^{-6}\nu^{-3.3}$ (5) and the commonly applied demarcation between swell and wind-sea of $\nu = 0.13$. Noting that the model data are drawn from every grid point in the spatial domain (excluding the TC eye) and hence every quadrant, it is in reasonably good agreement with the buoy data. Both the buoy and model are consistent with the fetch-limited result of Donelan et al. (1985) for $\nu > 0.13$. For $\nu < 0.13$ both the buoy data and model fall below the Donelan et al (1985) result, with the model apparently containing less energy at smaller values of non-dimensional frequency, ν (see Section 7). There are however limited buoy data for very small values of ν and the model values still lie within the data scatter of the buoys. For both the model and buoy data, a significant proportion of the data are for values of ν less than the swell wind-sea limit. This is consistent with the situation shown in Figure 1, where much of the wave field is dominated by remotely generated waves which propagate at phase speeds greater than the local wind speed.

Figures 4 and 5 show the one-dimensional spectrum, $E(f)$ and the directional spreading function, $D(f,\theta)$ for each quadrant of the TC for the cases of $V_{fm} = 2.5$ ms^{-1} and 5.0ms^{-1}, respectively. These results can be compared to the buoy data in Figure 1. As for the buoy observations, the model results show unimodal one-dimensional spectra throughout the spatial domain. There is some suggestion of bi-modality in the left rear quadrant for the case of $V_{fm} = 5.0$ms^{-1} (Figure 5). This same feature is seen for the buoy data in Figure 1. The vectors showing the peak wave

Accepted for publication in *Journal of Physical Oceanography*. DOI 10.1175/JPO-D-21-0005.1.

directions are similar for the two model cases, with both in good agreement with the buoy data.

As for the buoy data, the model spectra show a continuum of energy between the locally generated wind-sea and the remotely generated waves at the peak of the spectrum. This holds across all quadrants of the TC wave field and the model and buoy results are in reasonably good agreement. In addition to the model reproducing this continuum of energy, the rate at which the spectrum rotates from the wind direction to the direction of the remotely generated peak is also in good agreement with the buoy data. In the forward right quadrant, the rotation occurs (i.e. spectrum fully aligned with the wind) by $2f_p$ (buoy and model), where f_p is the frequency of the spectra peak. In the left forward quadrant, the rotation occurs by $2.5f_p$ (buoy and model). In the left rear quadrant, where the most confused wave conditions occur, there is some divergence between model ($1.5f_p$) and buoy ($2f_p$). In the right rear quadrant, buoy and model are again in good agreement ($1.5f_p$).

Interestingly, the model spectra appear narrower than the buoy spectra. The reason for this is not clear. It is perhaps that the analysis technique for the buoy data (Fourier expansion, Longuet-Higgins et al., 1963; Young, 1994) yields excessively broad spectra or that the nonlinear coupling between wind-sea and remotely generated waves in the DIA representation of the source term, S_{nl} in the model yields this result. It is unusual, as the DIA typically results in excessively broad spectra (Komen et al., 1984).

Accepted for publication in *Journal of Physical Oceanography*. DOI 10.1175/JPO-D-21-0005.1.

The results in Figures 2 to 5 add confidence that the WW3 model is reproducing the broad trends reported from measured buoy data for the TC wave field (noting the differences to the SRA data reported earlier). In addition, the model also appears to be able to capture the measured properties of the spectrum throughout the spatial wave field of the TC. This includes both the shape of the one-dimension spectrum, together with the directionally skewed spectra. As a result, the physics of the model, as represent by the propagation of energy and the energy balance of the source terms, S (6) within the model, produce results consistent with recorded data.

6. Energy balance in a translating tropical cyclones

Figures 6 and 7 show the source terms in the radiative transfer equation (6), $S(f,\theta)=S_{in}(f,\theta)+S_{nl}(f,\theta)+S_{ds}(f,\theta)$ for the two cases of $V_{fm}=2.5$ ms^{-1} and 5.0ms^{-1}, respectively. Because the magnitudes of the spectra and wind speeds vary for different regions of the tropical cyclones, the magnitudes of the source terms also vary. To display in a single figure, each of the source terms in Figures 6 and 7 have been normalized to have a maximum value of one.

Directly to the right of the TC centre, the wind and waves are more aligned than other regions of the TC and the source terms are similar to our understanding of the energy balance in fetch-limited growth (Komen et al., 1984). The atmospheric input, S_{in} is positive throughout the spectrum, including at the spectral peak. The dissipation, S_{ds} is approximately the mirror image of S_{in}, being negative across the spectrum. The nonlinear term, S_{nl} shows the characteristic plus-minus signature of this term (Komen et al., 1984), transferring energy from frequencies above the spectral peak to lower

Accepted for publication in *Journal of Physical Oceanography*. DOI 10.1175/JPO-D-21-0005.1.

frequencies, thus supporting growth of energy near the peak and its migration to lower frequencies.

As the mean wind direction and peak wave direction become separated in direction (e.g. left of TC centre), the energy balance becomes more complex. The atmospheric input, S_{in} is positive for the wind-sea (e.g. $f > 2f_p$). As the spectral peak is at a significant angle to the wind direction and often has a phase speed, $C > U_{10}$, S_{in} becomes negative at the spectral peak (opposing wind). The dissipation, S_{ds} is negative for all frequencies. As a result, both S_{in} and S_{ds} would result in decay of the remotely generated waves at the spectral peak. The nonlinear term, S_{nl} shows a plus-minus structure along the "ridge" of energy which joints the wind-sea spectrum at higher frequencies to the remotely-generated spectral peak at lower frequencies. This results in a cascade of energy from the wind-sea to the remotely-generated spectral peak components. Thus, although the spectral peak receives no direct positive input from the wind, it indirectly remains coupled to the wind by the energy cascade from the wind-sea. This continual flux of energy from the wind-sea to the remotely-generated spectral peak results in the continuum of energy between the two systems seen in the spectra in Figures 1, 4 and 5. Thus, the spectral peak acts in a "parasitic" manner, continually taking energy from the wind-sea and hence sustaining both the continuum of energy between the two systems and the sustained growth of the remotely generated spectra peak.

Even when the waves are separated by more than 90^0, this continual feed of energy from the wind-sea ensures the two systems remain connected. In none of the cases

Accepted for publication in *Journal of Physical Oceanography*. DOI 10.1175/JPO-D-21-0005.1.

shown in Figures 6 or 7 do the wind-sea and remotely-generated peak become decoupled systems and appear as separate spectral peaks.

As the spectra in Figures 4 and 5 and the source terms in Figures 6 and 7 are normalized, they do not provide information on the relative magnitudes of the source terms. In order to address this, Figure 8 shows the spectra and source terms for the case of $V_{fm} = 5 ms^{-1}$ and the octant to the NNW of the storm centre (Figure 5 for spectra and Figure 7 for source terms). In Figure 8, the terms are not normalized. Figure 8a shows the 1-D spectrum, $E(f)$ and Figure 8b the directional spectrum, $E(f,\theta)$, both have units of [m^2s]. The unimodal structure of the 1-D spectrum, as described above is clear, with the high frequency face being approximately proportional to f^{-4}. The directional spectrum, $E(f,\theta)$ clearly shows the low frequency peak at a frequency of approximately 0.07Hz and a direction of 118^0 (note only the directional spreading function, $D(f,\theta)$ was shown in Figure 5). This clearly seems to represent remotely generated waves propagating out from the intense wind regions of the tropical cyclone vortex. These waves are propagating at an angle of more than 90^0 to the local wind direction (216^0). The directional spectrum becomes directionally skewed, with high frequency components aligning with the local wind direction. However, both the 1-D and directional spectra remain unimodal.

The source terms, S_{in}, S_{nl} and S_{ds} are shown in Figures 8c, d, e (respectively) [units m^2] and the total source term $S_{tot}(f,\theta) = S_{in}(f,\theta) + S_{nl}(f,\theta) + S_{ds}(f,\theta)$, in Figure 8f. The results confirm the energy balance seen in the normalized results (i.e. the source terms are of similar magnitude). The wind input, S_{in} (Figure 8c) is positive for the

Accepted for publication in *Journal of Physical Oceanography*. DOI 10.1175/JPO-D-21-0005.1.

wind-sea and negative for the remotely generated waves at the spectral peak. That is, the peak is decaying as it is propagating at greater than 90^0 to the wind direction. The wind input in the region between the wind-sea and remotely generated waves (continuum of energy referred to above as the "ridge") is approximately zero, demonstrating that the local wind does not generate these waves. The dissipation, S_{ds} (Figure 8e) is, not surprisingly, negative for all components, being largest for the high frequency (steeper) components. Again, in the region between these two systems the dissipation is small.

The nonlinear term, S_{nl} (Figure 8d) is conservative, redistributing energy within the spectrum. It is clear that this term transfers energy from the wind-sea to the region of the "ridge", which joins the wind-sea and the remotely generated waves (Figure 8d). The nonlinear term is also negative at the spectral peak and appears to be transferring energy to frequencies lower than the spectral peak and at even increasing angles to the local wind direction. As seen in the spectrum in Figure 8b, this transfer from the peak results in a continued downshift in frequency and rotation in direction of the remotely generated peak. The total source term, S_{tot} (Figure 8f) in the "ridge" region between the wind-sea and the remotely generated peak is largely the same as S_{nl} (as the other source terms are approximately zero), confirming that the energy balance in this region is dominated by the nonlinear term. Hence, as noted above, it is the nonlinear term which is largely responsible for the "ridge" of energy between the wind-sea and remotely generated peak. Hence, it is S_{nl} which sustains the unimodal but skewed directional spectrum seen in both model and buoy data.

Accepted for publication in *Journal of Physical Oceanography*. DOI 10.1175/JPO-D-21-0005.1.

7. Discussion and conclusions

The results above show that the WW3 model is capable of reproducing the general features of the spectral shape throughout the spatial wave field of a TC. As a result, it is reasonable to assume that, to some level of accuracy, the source terms of the model capture the main physical processes active in this complex wave field. Importantly, the results confirm the speculation of Young (2006) and Tamizi and Young (2020) that the directionally-skewed spectra which result in such cases, are dominated by nonlinear energy transfer from the high-frequency wind-sea to the low-frequency remotely-generated spectral peak (Figure 8f). This coupling between the wind-sea and spectral peak is sustained even when the two systems are directionally separated by more than 90^0. Figure 9 shows a diagrammatic representation of the cascade of energy from the wind-sea, along the continuum of energy ("ridge") joining the wave systems to the spectral peak. This form of coupling across direction and frequency has been demonstrated for simpler systems by Young and van Vledder (1993). The present, results are, however, the first demonstration of such coupling in a tropical cyclone situation.

It is perhaps surprising, that even with the limitations of the DIA form of S_{nl}, the source term is still able to adequately model the interaction between the wind-sea and remotely generated waves that are essential to describing wave spectra within tropical cyclones. The fact that nonlinear interactions play such a critical role in shaping the TC spectrum, explains a number of observed features of such wave systems. Such features include: the skewed directional shape of the directional spectrum, and the fact that one-dimensional TC spectra are similar in shape to fetch-limited spectra, as well as the relationship between non-dimensional energy and non-dimensional frequency

Accepted for publication in *Journal of Physical Oceanography*. DOI 10.1175/JPO-D-21-0005.1.

and the observation that JONSWAP-type power laws can be used to predict significant wave height within TCs. All are results which rely on the self-similar properties of nonlinear interactions in shaping the wave spectrum (Young and Van Vledder, 1993).

As noted above, the DIA form for S_{nl} is a limitation of the present modelling approach. That limitation, together with differences in driving wind fields, probably account for the observed discrepancies between the model and observed spectra. In particular, Figure 3 shows that model spectra seem to have less energy at low frequencies than observed spectra. This suggests that the model underestimates the energy in the “parasitic” remotely-generated spectral peak. It is possible that the energy input in the intense wind regions of the TC are underestimated. After all, S_{in} has never been measured under TC conditions and hence this term is extrapolated to these wind speeds. This may result in an underestimation of the remotely generated energy. Noting the important role of S_{nl} in defining the spectral shape, it is more likely that the magnitude of the energy cascade to the spectral peak is underestimated by the model. As the DIA considers only a very small subset of interacting wave components (Komen et al., 1984), it is plausible that the magnitude of the energy transfer is larger than shown in these calculations.

Despite these limitations, the present results have clearly shown that nonlinear interactions are critical in wind-wave evolution in tropical cyclones. The results are also a compelling validation of the central role that Hasselmann’s quadruplet interactions play in the dynamics of wind waves in a wide range of forcing scenarios (Hasselmann, 1962).

Accepted for publication in *Journal of Physical Oceanography*. DOI 10.1175/JPO-D-21-0005.1.

Acknowledgements

The authors would like to acknowledge the support provide to AT by the University of Melbourne through a PhD scholarship. We also thank the US National Oceanic and Atmospheric Administration (NOAA) for providing access to HPC resources.

Accepted for publication in *Journal of Physical Oceanography*. DOI 10.1175/JPO-D-21-0005.1.

8. References

Ardhuin, F., E. Rogers, A. Babanin, J-F. Filipot, R. Magne, A. Roland, A. Van Der Westhuysen, P. Queffeulou, J-M. Lefevre, L. Aouf and F. Collard: 2010. Semi-empirical dissipation source functions for ocean waves: part I, definition, calibration and validation. *J. Phys. Oceanogr.*, **40**, 1917–1941. doi: 10.1175/ 2010JPO4324.1 .

Babanin, A.V., M.L. Banner, I.R. Young and M.A. Donelan, 2007: Wave follower field measurements of the wind input spectral function. Part III: Parameterization of the wind input enhancement due to wave breaking. *J. Phys. Oceanogr.*, **37**, 11, 2764-2775.

Babanin, A.V. , 2011: Breaking and Dissipation of Ocean Surface Waves. *Cambridge University Press*.

Beal, R.C., T.W. Gerling, D.E. Irvine, F.M. Monaldo and D.G. Tilley, 1986: Spatial variations of ocean wave directional spectra from the Seasat synthetic aperture radar, *J. Geophys. Res*., **91**, 2433–2449.

Bidlot, J.-R. , 2012: Present status of wave forecasting at E.C.M.W.F. In: *ECMWF-Work- shop on Ocean Waves*, Shinfield Park, Reading, RG2 9AX, United Kingdom, p16.

Bidlot, J.-R. , P. Janssen and S. Abdalla, 2007: A Revised Formulation of Ocean Wave Dissipation and its Model Impact. Technical Report 509, *European Centre for Medium-Range Weather Forecasts*, Shinfield Park, Reading, RG2 9AX, England .

Accepted for publication in *Journal of Physical Oceanography*. DOI 10.1175/JPO-D-21-0005.1.

Black, J.L., 1979: Hurricane Eloise directional wave energy spectra, *Proceedings of the Offshore Technology Conference*, Houston, TX, USA, 30 April–3 May, OTC 3594.

Black, P.G., E.A. D'Asaro, W.M. Drennan, J.R. French, P.P. Niiler, T.B. Sanford, E.J. Terrill, E.J. Walsh and J.A. Zhang, 2007: Air-sea exchange in hurricanes: Synthesis of observations from the coupled boundary layer air-sea transfer experiment, *Bull. Am. Meteorol. Soc*., **88**, 357–374.

Bretschneider, C.L., 1972: A non-dimensional stationary hurricane wave model. In *Proceedings of the Fourth Offshore Technology Conference*, Houston, TX, USA, 1–3 May.

Cavaleri, L., J-H.G.M. Alves, F. Ardhuin, A. Babanin, M. Banner, K. Belibassakis, M. Benoit, M. Donelan, J. Groeneweg, T.H.C. Herbers, P. Hwang, P.A.E.M., Janssen, T. Janssen, I.V. Lavrenov, R. Magne, J. Monbaliu, M. Onorato, V. Polnikov, D. Resio, W.E. Rogers, A. Sheremet, J. McKee-Smith, H.L. Tolman, G. van Vledder, J. Wolf and I. Young, 2007: Wave modelling - the state of the art. *Prog. Oceanogr*., **75** (4), 603–674. doi: 10.1016/j.pocean.20 07.05.0 05

Collins, C.O., H. Potter, B. Lund, H. Tamura and H. C. Graber, 2018: Directional Wave Spectra Observed During Intense Tropical Cyclones, *J. Geophy. Res*., **123**, 773-793.

Accepted for publication in *Journal of Physical Oceanography*. DOI 10.1175/JPO-D-21-0005.1.

Donelan, M., M. Hamilton and W. Hui, 1985: Directional Spectra of Wind-Generated waves. *Phil. Trans. of Royal Society*, **A315**, 509-562.

Donelan, M.A., A.V. Babanin, I.R. Young and M.L. Banner, M.L., 2006: Wave-Follower field measurements of the wind-input spectral function. Part II: parameterization of the wind input. *J. Phys. Oceanogr*., **36** (8), 1672–1689. doi: 10.1175/JPO2933.1 .

Elachi, C., T.W. Thompson and D.B. King, 1977: Observations of the ocean wave pattern under Hurricane Gloria with synthetic aperture radar, *Science*, **198**, 609–610.

Evans, D., C. L. Conrad and F. M. Paul, 2003: *Handbook of automated data quality control checks and procedures of the National Data Buoy Center*. NOAA/National Data Buoy Center Tech. Doc. 03-02, 44 pp.

Gonzalez, F.I., T.E. Thompson, W.E. Brown and D.E. Weissman, 1978: Seasat wind and wave observations of Northeast Pacific Hurricane Iva, 13 August 1978, *J. Geophys. Res.*, **87**, 3431–3438.

Hasselmann, K., T.P. Barnett, E. Bouws, H. Carlson, D.E. Cartwright, K, Enke, J.A. Ewing, H. Gienapp, D.E. Hasselmann, P. Kruseman, et al., 1973: Measurements of wind-wave growth and swell decay during the Joint North SeaWave Project (JONSWAP), In Hydraulic Engineering Reports; *Deutches Hydrographisches Institute*: Hamburg, Germany, 95pp.

Accepted for publication in *Journal of Physical Oceanography*. DOI 10.1175/JPO-D-21-0005.1.

Hasselmann, S., K. Hasselmann, J.H. Allender, T.P. Barnett, 1985: Computations and parameterizations of the nonlinear energy transfer in a gravity-wave spectrum. Part II: parameterizations of the nonlinear energy transfer for application in wave models. *J. Phys. Oceanogr.*, **15** (11), 1378–1392.

Hasselmann, K. , 1962: On the non-linear energy transfer in a gravity-wave spectrum Part 1. General theory. *J. Fluid Mech.* **12**, 481–500 .

Holland, G.J., 1980: An analytical model of the wind and pressure profiles in hurricanes, *Mon. Weather Rev*., **108**, 1212–1218.

Holland, G., 2008: A Revised Hurricane Pressure–Wind Model. *Mon. Wea. Rev*., **136**, 3432-3445.

Holland, G.J., J.I. Belanger and A. Fritz, 2010: A Revised Model for Radial Profiles of Hurricane Winds, *Monthly Weather Rev*., **138**, 4393-4401.

Holt, B. and F.I. Gonzalez, 1986: SIR-B observations of dominant ocean waves near hurricane Josephine, *J. Geophys. Res*., **91**, 8595–8598.

Hu, K. and Q. Chen, 2011: Directional spectra of hurricane-generated waves in the Gulf of Mexico, *Geophys. Rev. Lett*., **38**, L19608.

Accepted for publication in *Journal of Physical Oceanography*. DOI 10.1175/JPO-D-21-0005.1.

Hwang, P.A., 2016: Fetch- and duration-limited nature of surface wave growth inside tropical cyclones: With applications to air-sea exchange and remote sensing, *J. Phys. Oceanogr*., **46**, 41–56.

Hwang, P.A. and E.J. Walsh, 2016: Azimuthal and radial variation of wind-generated surface waves inside tropical cyclones, *J. Phys. Oceanogr*., **46**, 2605–2621.

Hwang, P.A. and Y. Fan, 2017: Effective fetch and duration of tropical cyclone wind fields estimated from simultaneous wind and wave measurements: Surface wave and air-sea exchange computation, *J. Phys. Oceanogr*., **47**, 447–470.

Hwang, P.A., Y. Fan, F.J. Ocampo-Torres and H. García-Nava, 2017: Ocean Surface Wave Spectra inside Tropical Cyclones, *J. Phys. Oceanogr*., **47**, 2393-2417. doi: 10.1175/JPO-D-17-0066.1

Hwang, P.A. and E.J. Walsh, 2018a: Propagation Directions of Ocean Surface Waves inside Tropical Cyclones, *J. Phys. Oceanogr*., **48**, 1495-1511. doi: 10.1175\JPO-D-18-0015.1.

Hwang, P.A. and E.J. Walsh, 2018b: Estimating Maximum Significant Wave Height and Dominant Wave Period inside Tropical Cyclones, *Wea. Forecasting*, **33**, 955-966. doi:10.1175\WAF-D-17-0186.1

Janssen, P.A.E.M. , 2004: The Interaction of Ocean Waves and Wind. Cambridge University Press .

Accepted for publication in *Journal of Physical Oceanography*. DOI 10.1175/JPO-D-21-0005.1.

Janssen, P.A.E.M., 1991: Quasi-linear theory of wind-wave generation applied to wave forecasting. *J. Phys. Oceanogr*., **21** (11), 1631–1642.

King, D.B. and O.H. Shemdin, 1987: Radar observations of hurricane wave directions, *16th International Conf. Coastal Engineering*, Hamburg, Germany, ASCE, 209–226.

Klotz, B.W. and H. Jiang, 2016: Global composites of surface wind speeds in tropical cyclones based on a 12year scatterometer database. *Geophy. Res. Lett*., **43**, 10,480–10,488.

Klotz, B.W. and H. Jiang, 2017: Examination of Surface Wind Asymmetries in Tropical Cyclones. Part I: General Structure and Wind Shear Impacts. *Mon. Wea. Rev.*, **145**, 3989-4009.

Komen, G.J., S. Hasselmann and K. Hasselmann, 1984: On the existence of a fully developed wind-sea spectrum, *J. Phys. Oceanogr*., **14**, 1271-1284.

Longuet-Higgins, M.S., D.E. Cartwright and N.D. Smith, 1963: Observations of the directional spectrum of sea waves using the motion of a floating buoy. In *Ocean Wave Spectra*, Prentice-Hall, 111-136.

Accepted for publication in *Journal of Physical Oceanography*. DOI 10.1175/JPO-D-21-0005.1.

Leckler, F., F. Ardhuin, J.F. Filipot and A. Mironov, 2013: Dissipation source terms and whitecap statistics. *Ocean Modell.*, **70**, 62–74. doi: 10.1016/j.ocemod.2013.03.007 .

Liu, Q., A. Babanin, Y. Fan, S. Zieger, C. Guan, Il-J. Moon, 2017: Numerical simulations of ocean surface waves under hurricane conditions: Assessment of existing model performance. *Ocean Modell.*, **118**, 73-93.

McLeish, W. and D.B. Ross, 1983: Imaging radar observations of directional properties of ocean waves, *J. Geophys. Res.*, **88**, 4407–4419,

Moon, I.-J., I. Ginis, and T. Hara, 2003: Numerical simulation of sea surface directional wave spectra under typhoon wind forcing. *J. Phys. Oceanogr.*, **33** (8), 1680–1706. doi: 10.1016/S10 01-6058(09)60 015-9 .

Ochi, M.K. and M.H. Chiu, 1982: Nearshore wave spectra measured during Hurricane David, *Proceedings of the 18th International Confession on Coastal Engineering*, Cape Town, South Africa, 14–19 November, ASCE: Hamburg, Germany, 77–86.

Ochi, M.K, 1993: On hurricane-generated seas, *Proceedings of the 2nd International Symposium on Ocean Wave Measurement and Analysis*, New Orleans, LA, USA, 25–28 July, ASCE, 374–387.

Accepted for publication in *Journal of Physical Oceanography*. DOI 10.1175/JPO-D-21-0005.1.

Olfateh, M., D. P. Callaghan, P. Nielsen, and T. E. Baldock, 2017: Tropical Cyclone asymmetry - development and evaluation of a new parametric model. *J. Geophys. Res.*, **122**, 458–469.

Patterson, M.M., 1974: Oceanographic data from Hurricane Camille, *Proceedings of the Offshore Technology Conference*, Houston, TX, USA, 6–8 May, OTC-2109-MS.

Perrie, W., B. Toulany, D.T. Resio, A. Roland, J.P. Auclair, J.P., 2013: A two-scale approximation for wave-wave interactions in an operational wave model. *Ocean Modell.* **70**, 38–51. doi: 10.1016/j.ocemod.2013.06.008 .

Powell, M. D., 1982: The transition of the Hurricane Frederic boundary-layer wind field from the open Gulf of Mexico to landfall. *Mon. Wea. Rev.*, **110**, 1912–1932.

Resio, D.T. and W. Perrie, 2008: A two-scale approximation for efficient representation of nonlinear energy transfers in a wind wave spectrum. Part I: theoretical development. *J. Phys. Oceanogr*. **38** (12), 2801–2816 .

Rogers, E.W., A.V. Babanin and D.W. Wang, D.W., 2012. Observation-consistent input and whitecapping dissipation in a model for wind-generated surface waves: description and simple calculations. *J. Atmos. Oceanic Technol*. **29** (9), 1329–1346. doi: 10.1175/JTECH- D- 11- 0 0 092.1 .

Accepted for publication in *Journal of Physical Oceanography*. DOI 10.1175/JPO-D-21-0005.1.

Rogers, W. E., and G. P. van Vledder, 2013: Frequency width in predictions of windsea spectra and the role of the nonlinear solver. *Ocean Modell.*, **70**, 52–61, doi:10.1016/j.ocemod.2012.11.010.

Ross, D.B., 1976: A simplified model for forecasting hurricane generated waves, *Bull. Am. Meteorol. Soc*., 113–115.

Tamizi, A. and I.R. Young, 2020: The spatial distribution of ocean waves in tropical cyclones. *Jnl. Phys. Oceang*., **50**, 2123-2139. doi: 10.1175/JPO-D-20-0020.1.

Tamizi, A., I.R. Young, A. Ribal and J-H. Alves 2020: Global scatterometer observations of the structure of tropical cyclone wind fields”, *Mon. Wea. Rev*., **148**, 4673-4692. doi: 10.1175/MWR-D-20-0196.1.

Tolman, H.L., 1991: A third-generation model for wind waves on slowly varying, unsteady, and inhomogeneous depths and currents. *J. Phys. Oceanogr*., **21** (6), 782–797.

Tolman, H. , 2002: Validation of WAVEWATCH III Version 1.15 for a Global Domain. Technical Report 213, *Environmental Modeling Center*, Ocean Modeling Branch .

Tolman, H.L. and J-H.G.M Alves, 2005: Numerical modeling of wind waves generated by tropical cyclones using moving grids, *Ocean Modelling*, **9**, 305–323.

Accepted for publication in *Journal of Physical Oceanography*. DOI 10.1175/JPO-D-21-0005.1.

Tolman, H.L., 2013: A generalized multiple discrete interaction approximation for resonant four-wave interactions in wind wave models. *Ocean Modell*. **70**, 11–24. doi: 10.1016/j.ocemod.2013.02.005 .

U.S. Army Corp of Engineers, 1977: *Shore Protection Manual: Volume I,II,III—Three Volumes*, U.S. Army Coastal Engineering Research Center: Vicksburg, MS, USA.

Walsh, E.J. et al., 2002: Hurricane directional wave spectrum spatial variation at landfall. *J. Phys. Oceanogr.*, **32**, 1667-1684.

Walsh, E.J., C. W. Fairall and I. PopStefanija, 2021: In the eye of the storm. *J. Phys. Oceanogr*. (in press).

WAVEWATCH III ® Development Group (WW3DG), 2019: User manual and system documentation of WAVEWATCH III ® version 6.07. Tech. Note 333, NOAA/NWS/NCEP/MMAB, College Park, MD, USA. 465 pp. + Appendices.

Whalen, J.E. and M.K. Ochi, 1978: Variability of wave spectral shapes associated with hurricanes, *Proceedings of the Offshore Technology Conference*, Houston, TX, USA, 8–11 May, OTC3228.

Willoughby, H. E., R. W. R. Darling, and M. E. Rahn, 2006: Parametric representation of the primary hurricane vortex. Part II: A new family of sectionally continuous profiles, *Mon. Wea. Rev.*, **134**, 1102–1120.

Accepted for publication in *Journal of Physical Oceanography*. DOI 10.1175/JPO-D-21-0005.1.

Wright, C.W., E.J. Walsh, D. Vandemark, W.B. Krabill, A.W. Garcia, S.H. Houston, M.D. Powell, P.G. Black and F.D. Marks, 2001: Hurricane directional wave spectrum spatial variation in the open ocean, *J. Phys. Oceanogr*., **31**, 2472–2488

Young, I.R. and G.P. Burchell, 1986: Hurricane generated waves as observed by satellite, *Ocean Eng*., **23**, 761–776.

Young, I.R., 1988a: A Parametric Hurricane Wave Prediction Model, *ASCE Jnl. of Waterway, Port, Coastal and Ocean Engineering*, **114**, 5, 637-652.

Young, I.R., 1988b: A Shallow Water Spectral Wave Model. *Jnl. of Geophysical Research*, **93**, C5, 5113-5129.

Young, I.R. and G.Ph. van Vledder, 1993: A Review of the Central Role of Nonlinear Interactions in Wind-Wave Evolution, *Phil. Trans. Roy. Soc. Lond. A* , **342**, 505-524.

Young, I.R., 1994: On the Measurement of Directional Wave Spectra, *Applied Ocean Research*, **16**, 283-294.

Young, I.R., 1998: Observations of the spectra of hurricane generated waves, *Ocean Eng.*, **25**, 261–276.

Young, I.R., 2006: Directional spectra of hurricane wind-waves, *J. Geophys. Res*., **111**, C08020, doi:10.1029/2006JC003540.

Accepted for publication in *Journal of Physical Oceanography*. DOI 10.1175/JPO-D-21-0005.1.

Young, I.R. and J. Vinoth, 2013, An ‘extended fetch’ model for the spatial distribution of tropical cyclone wind-waves as observed by altimeter, *Ocean Eng*., **70**, 14–24.

Young, I.R., 2017: A Review of Parametric Descriptions of Tropical Cyclone Wind-Wave Generation, *Atmosphere*, **8**, 194; doi:10.3390/atmos8100194.

Zhang, J., and E. W. Uhlhorn, 2012: Hurricane sea surface inflow angle and an observation-based parametric model. *Mon. Wea. Rev*., **140**, 3587–3605.

Zieger, S., A.V. Babanin, W.E. Rogers and I.R. Young, 2015: Observation-based source terms in the third-generation wave model WAVEWATCH. *Ocean Modell*. **218**, 1–24. doi: 10.1016/j.ocemod.2015.07.014 .

Accepted for publication in *Journal of Physical Oceanography*. DOI 10.1175/JPO-D-21-0005.1.

Figure Captions

Figure 1. Directional spectra within tropical cyclones from the in-situ data of Tamizi and Young (2020). Data presented for locations shown by the dots in each octant of the storm which is propagating to the north (up the page). Solid arrows (and vertical lines) show mean wind direction and dashed arrows (and vertical lines) the peak wave direction. At each point the directional spreading function, $D(f,\theta)$ and the one-dimensional spectrum, $E(f)$ is shown. Both $D(f,\theta)$ and $E(f)$ have been normalized, such that they have maximum values of one. All angles measured anti-clockwise from x axis.

Figure 2. Contour plots of significant wave height, H_s within tropical cyclones. Also shown are vectors of the peak wave direction. The spatial scale is normalized by the radius to maximum winds, R_m. (a) Tropical cyclone velocity of forward movement, $V_{fm} = 2.5\text{ms}^{-1}$, (b) $V_{fm} = 5.0\text{ms}^{-1}$.

Figure 3. Non-dimensional energy, ε as a function of non-dimensional frequency, ν for waves within tropical cyclones. (a) In-situ buoy data of Tamizi and Young (2020) (b) WW3 model for the case of a tropical cyclone with $\Delta p = 50\text{HPa}$ and $V_{fm} = 2.5\text{ms}^{-1}$.

Figure 4. Directional spectra within a tropical cyclone from the WW3 model. Data presented for locations shown by the dots in each octant of the storm which is propagating to the north (up the page). Solid arrows (and vertical lines) show mean wind direction and dashed arrows (and vertical lines) the peak wave direction. At each point the directional spreading function, $D(f,\theta)$ and the one-dimensional spectrum, $E(f)$ is shown. Both $D(f,\theta)$ and $E(f)$ have been normalized, such that they have maximum values of one. Case shown has $\Delta p = 50\text{HPa}$ and $V_{fm} = 2.5\text{ms}^{-1}$. All angles measured anti-clockwise from x axis.

Figure 5. Directional spectra within a tropical cyclone from the WW3 model. Data presented for locations shown by the dots in each octant of the storm which is propagating to the north (up the page). Solid arrows (and vertical lines) show mean wind direction and dashed arrows (and vertical lines) the peak wave direction. At each point the directional spreading function, $D(f,\theta)$ and the one-dimensional spectrum, $E(f)$ is shown. Both $D(f,\theta)$ and $E(f)$ have been normalized, such that they have maximum values of one. Case shown has $\Delta p = 50\text{HPa}$ and $V_{fm} = 5.0\text{ms}^{-1}$. All angles measured anti-clockwise from x axis.

Figure 6. Source terms for the directional spectra shown in Figure 4. At each location, the atmospheric input, S_{in}, nonlinear interaction, S_{nl} and dissipation, S_{ds} are shown. Each source term has been normalized to have an absolute maximum value of one. Normalized energy levels are shaded with red for positive and blue for negative. Case

Accepted for publication in *Journal of Physical Oceanography*. DOI 10.1175/JPO-D-21-0005.1.

shown has $\Delta p = 50$HPa and $V_{fm} = 2.5$ms^{-1}. Solid vertical lines show mean wind direction and dashed vertical lines the peak wave direction. All angles measured anti-clockwise from x axis.

Figure 7. Source terms for the directional spectra shown in Figure 5. At each location, the atmospheric input, S_{in}, nonlinear interaction, S_{nl} and dissipation, S_{ds} are shown. Each source term has been normalized to have an absolute maximum value of one. Normalized energy levels are shaded with red for positive and blue for negative. Case shown has $\Delta p = 50$HPa and $V_{fm} = 5.0$ms^{-1}. Solid vertical lines show mean wind direction and dashed vertical lines the peak wave direction. All angles measured anti-clockwise from x axis.

Figure 8. WW3 model directional spectra and source terms from a location in the NNW octant of a tropical cyclone with $\Delta p = 50$HPa and $V_{fm} = 5.0$ms^{-1}. (a) One dimensional spectrum, $E(f)$ (m^{2}s), (b) Directional spectrum, $E(f,\theta)$ (m^{2}s), contours drawn at [0.1, 0.5, 1, 5, 10, 50, 100, 200], (c) Wind input source term, $S_{in}(f,\theta)$ x10^3 (m^2), (d) Nonlinear source term, $S_{nl}(f,\theta)$ x10^3 (m^2), (e) Dissipation source term, $S_{ds}(f,\theta)$ x10^3 (m^2), (f) Total source term, $S_{tot}(f,\theta)$ x10^3 (m^2). For each panel, the vertical solid line shows the wind direction and the dashed line the peak wave direction. All angles measured anti-clockwise from x axis.

Figure 9. An example of the role played by the nonlinear term, S_{nl} in tropical cyclone wave evolution. The nonlinear term transfers energy form the wind-sea to remotely generated waves at the spectral peak. This occurs through an energy cascade along the "ridge" connecting these wave systems. As a result, the waves at the spectral peak act in a "parasitic" manner to take energy for the local wind-sea to enhance growth at the spectral peak. The process ensures that the two wave systems remain connected through the directionally skewed spectrum. The case shown is for the spectrum in the west-south-west octant of Figure 4.

Accepted for publication in *Journal of Physical Oceanography*. DOI 10.1175/JPO-D-21-0005.1.

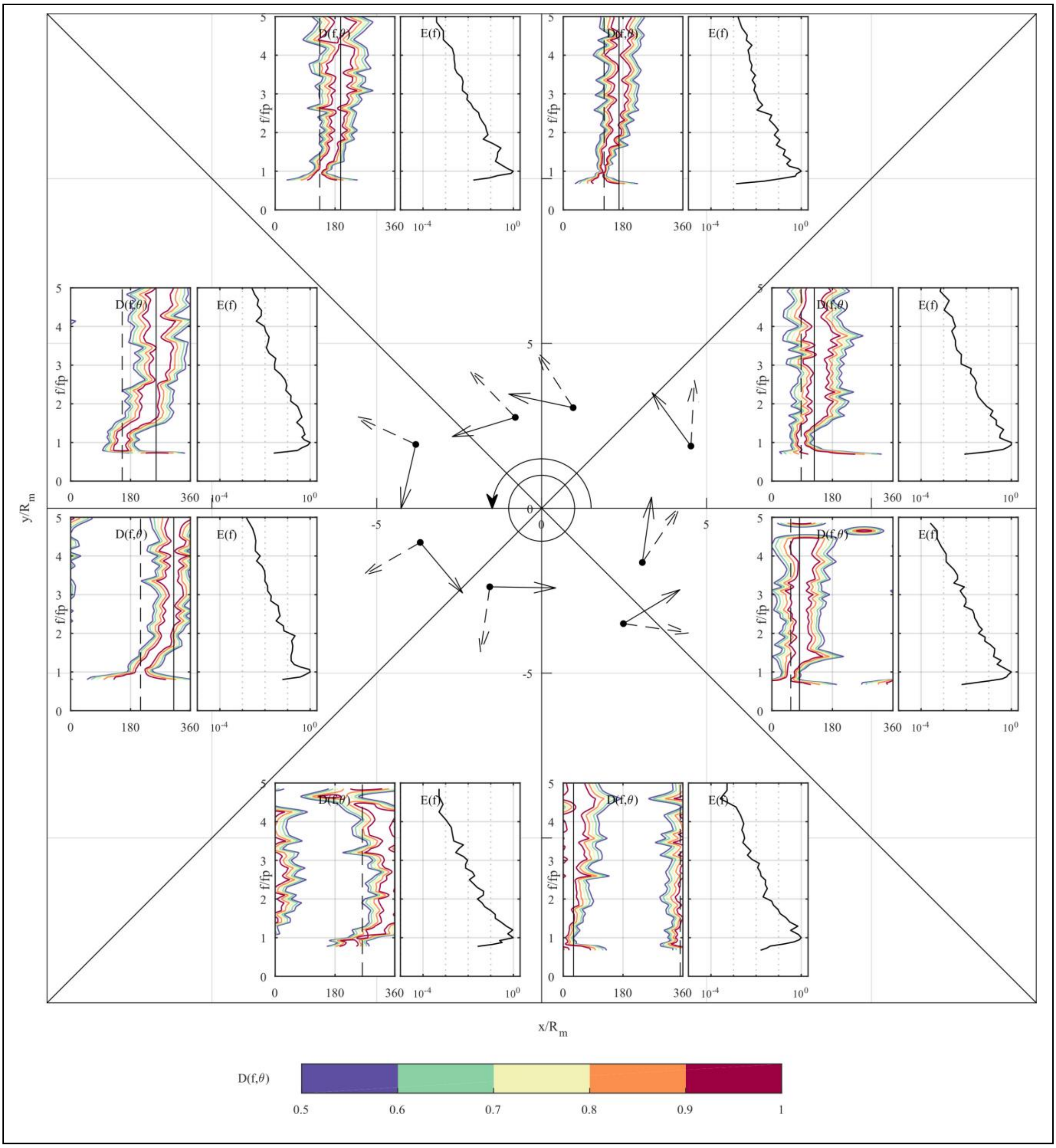

Figure 1. Directional spectra within tropical cyclones from the in-situ data of Tamizi and Young (2020). Data presented for locations shown by the dots in each octant of the storm which is propagating to the north (up the page). Solid arrows (and vertical lines) show mean wind direction and dashed arrows (and vertical lines) the peak wave direction. At each point the directional spreading function, $D(f,\theta)$ and the one-dimensional spectrum, $E(f)$ is shown. Both $D(f,\theta)$ and $E(f)$ have been normalized, such that they have maximum values of one. All angles measured anti-clockwise from x axis.

Accepted for publication in *Journal of Physical Oceanography*. DOI 10.1175/JPO-D-21-0005.1.

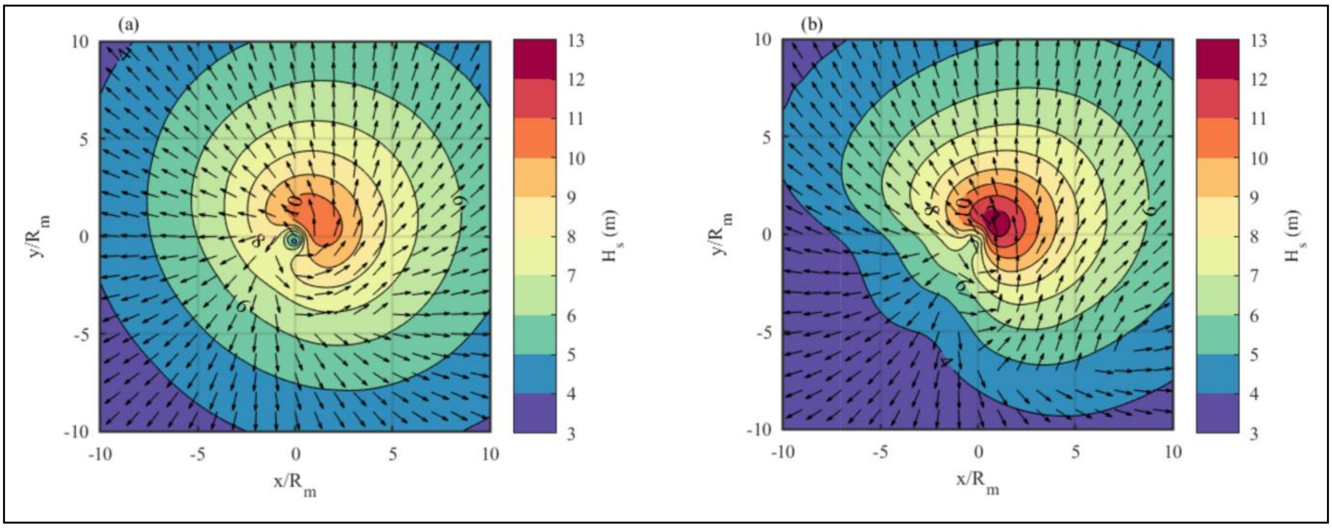

Figure 2. Contour plots of significant wave height, H_s within tropical cyclones. Also shown are vectors of the peak wave direction. The spatial scale is normalized by the radius to maximum winds, R_m. (a) Tropical cyclone velocity of forward movement, $V_{fm} = 2.5\text{ms}^{-1}$, (b) $V_{fm} = 5.0\text{ms}^{-1}$.

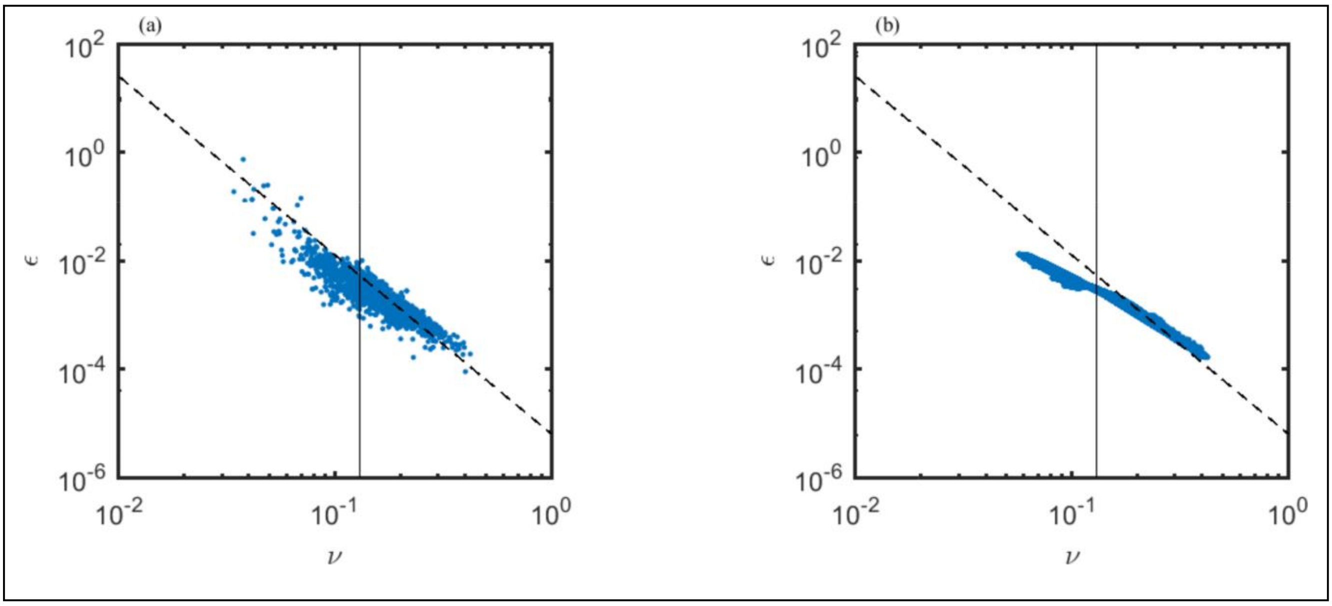

Figure 3. Non-dimensional energy, ε as a function of non-dimensional frequency, ν for waves within tropical cyclones. (a) In-situ buoy data of Tamizi and Young (2020) (b) WW3 model for the case of a tropical cyclone with $\Delta p = 50\text{HPa}$ and $V_{fm} = 2.5\text{ms}^{-1}$.

Accepted for publication in *Journal of Physical Oceanography*. DOI 10.1175/JPO-D-21-0005.1.

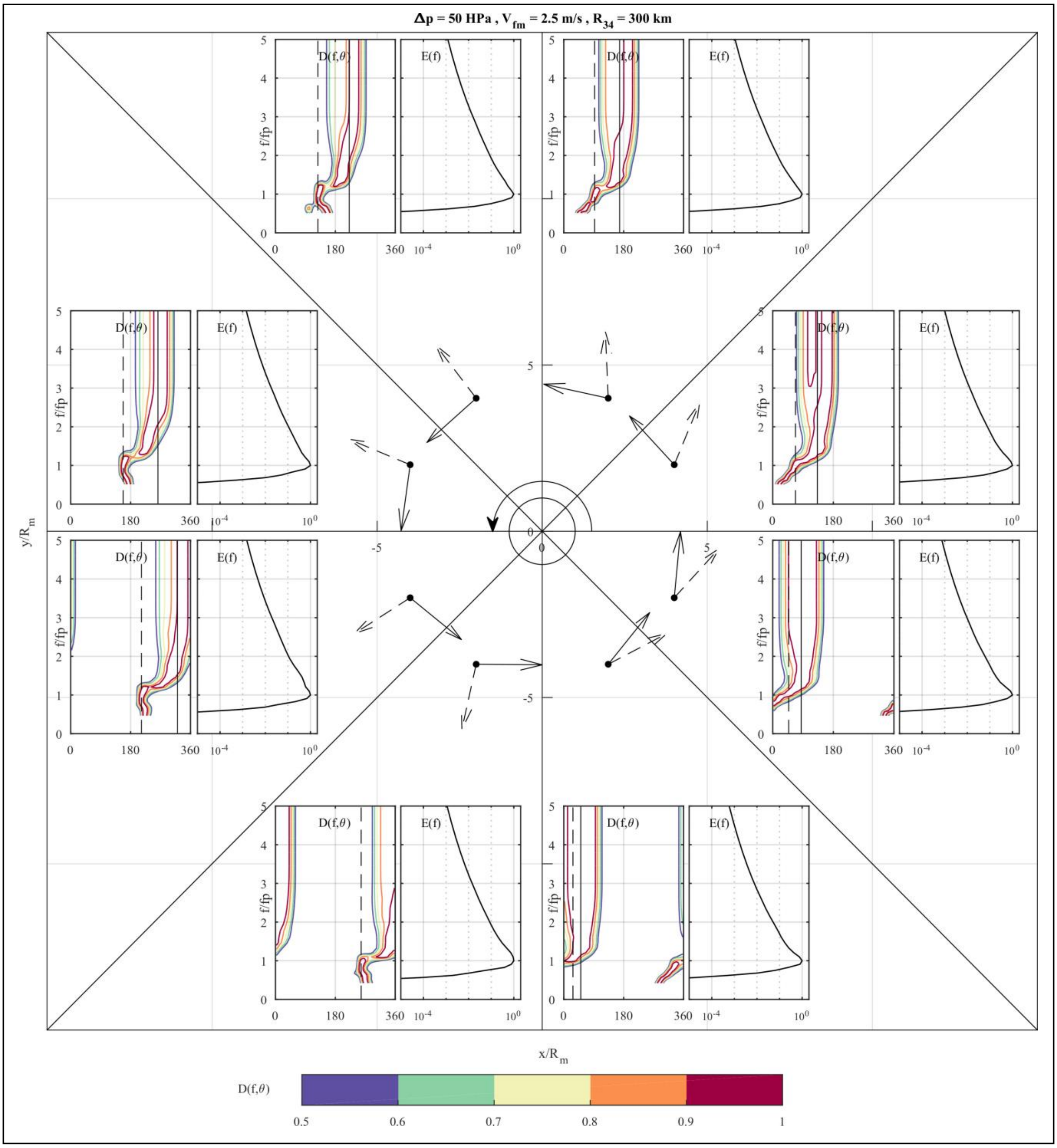

Figure 4. Directional spectra within a tropical cyclone from the WW3 model. Data presented for locations shown by the dots in each octant of the storm which is propagating to the north (up the page). Solid arrows (and vertical lines) show mean wind direction and dashed arrows (and vertical lines) the peak wave direction. At each point the directional spreading function, $D(f,\theta)$ and the one-dimensional spectrum, $E(f)$ is shown. Both $D(f,\theta)$ and $E(f)$ have been normalized, such that they have maximum values of one. Case shown has $\Delta p = 50$HPa and $V_{fm} = 2.5$ms^{-1}. All angles measured anti-clockwise from x axis.

943

Accepted for publication in *Journal of Physical Oceanography*. DOI 10.1175/JPO-D-21-0005.1.

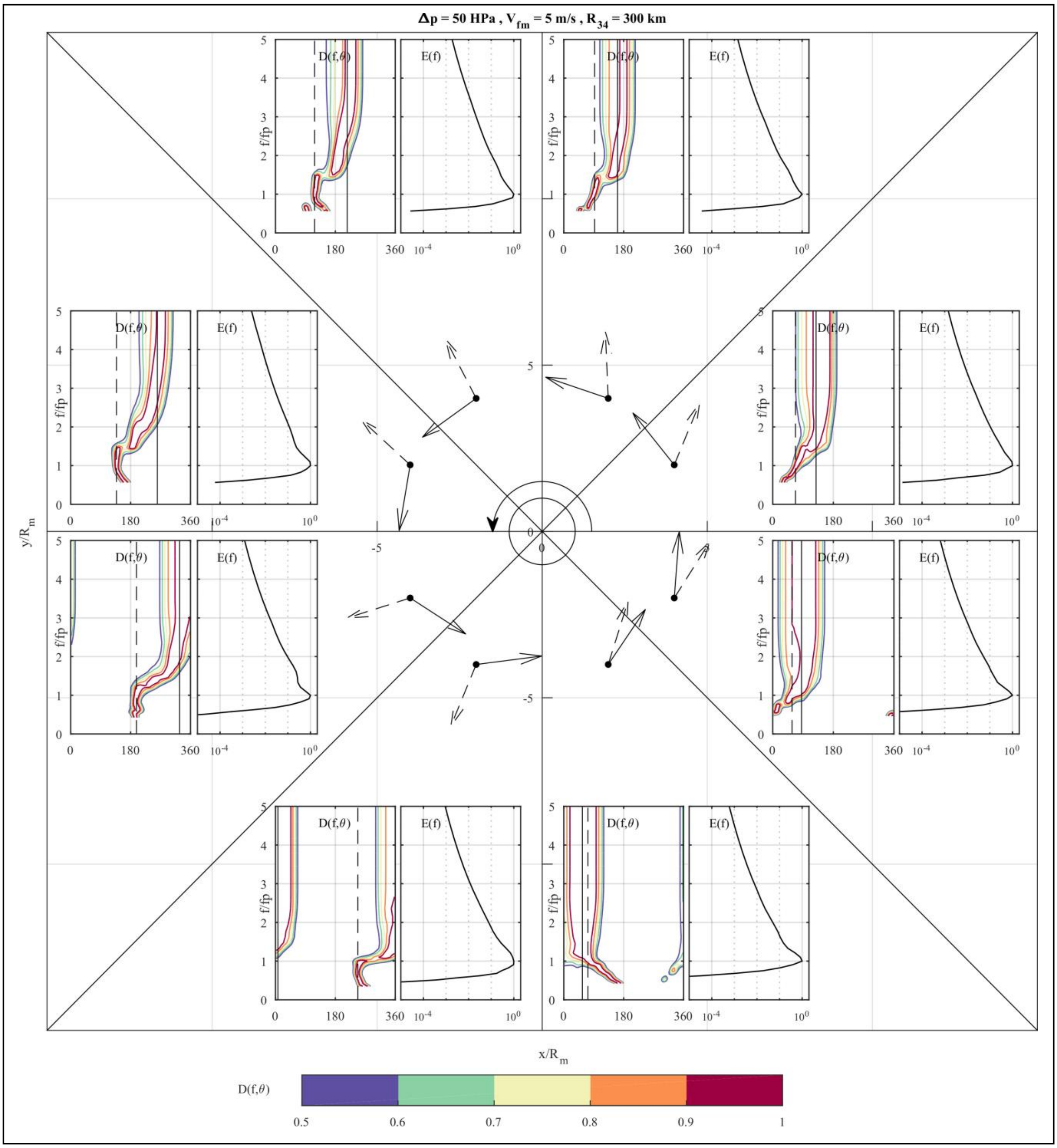

Figure 5. Directional spectra within a tropical cyclone from the WW3 model. Data presented for locations shown by the dots in each octant of the storm which is propagating to the north (up the page). Solid arrows (and vertical lines) show mean wind direction and dashed arrows (and vertical lines) the peak wave direction. At each point the directional spreading function, $D(f,\theta)$ and the one-dimensional spectrum, $E(f)$ is shown. Both $D(f,\theta)$ and $E(f)$ have been normalized, such that they have maximum values of one. Case shown has $\Delta p = 50$HPa and $V_{fm} = 5.0\text{ms}^{-1}$. All angles measured anti-clockwise from x axis.

Accepted for publication in *Journal of Physical Oceanography*. DOI 10.1175/JPO-D-21-0005.1.

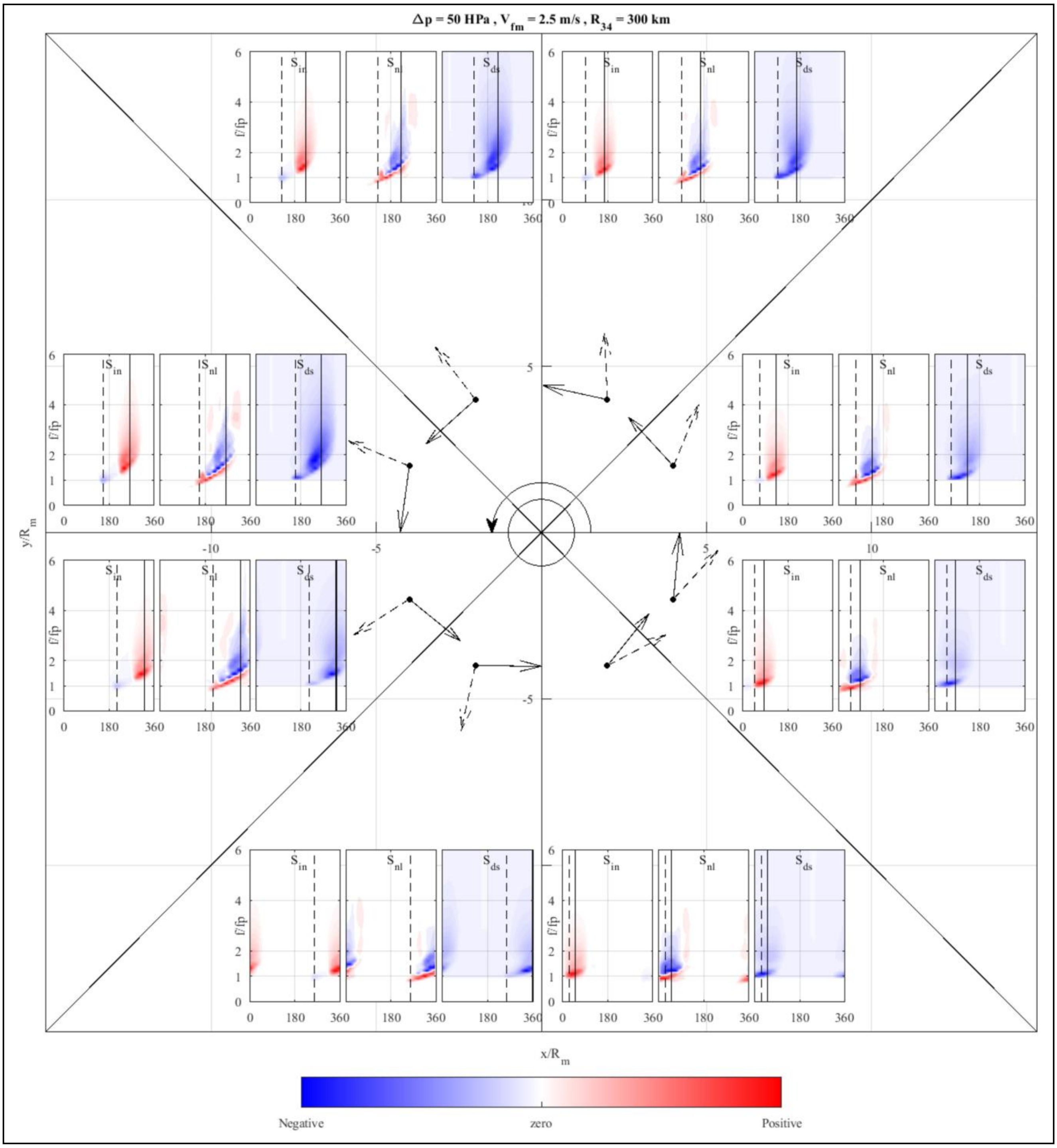

946

Figure 6. Source terms for the directional spectra shown in Figure 4. At each location, the atmospheric input, S_{in}, nonlinear interaction, S_{nl} and dissipation, S_{ds} are shown. Each source term has been normalized to have an absolute maximum value of one. Normalized energy levels are shaded with red for positive and blue for negative. Case shown has $\Delta p = 50$HPa and $V_{fm} = 2.5$ms^{-1}. Solid vertical lines show mean wind direction and dashed vertical lines the peak wave direction. All angles measured anti-clockwise from x axis.

947

948

Accepted for publication in *Journal of Physical Oceanography*. DOI 10.1175/JPO-D-21-0005.1.

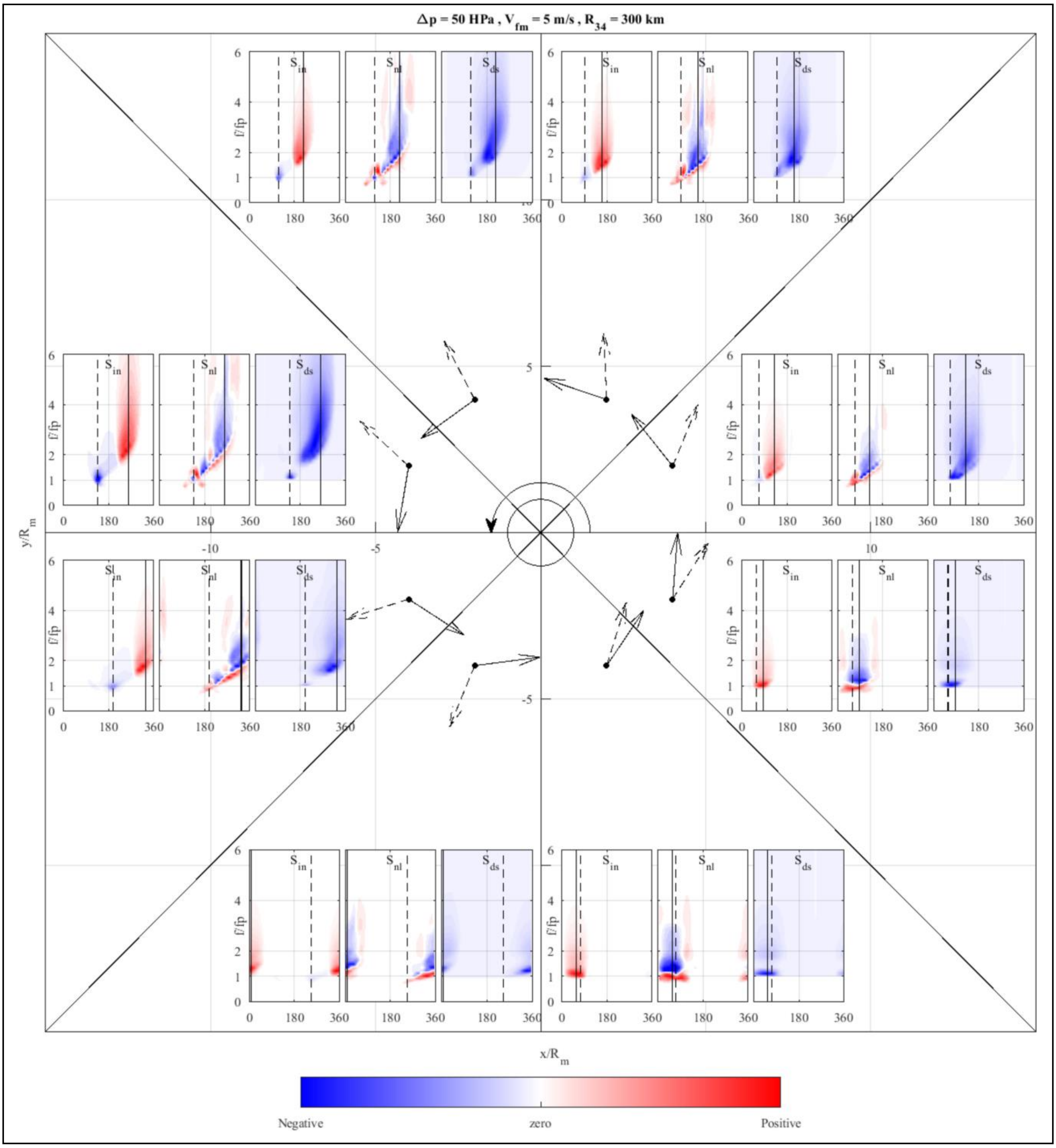

949

Figure 7. Source terms for the directional spectra shown in Figure 5. At each location, the atmospheric input, S_{in}, nonlinear interaction, S_{nl} and dissipation, S_{ds} are shown. Each source term has been normalized to have an absolute maximum value of one. Normalized energy levels are shaded with red for positive and blue for negative. Case shown has $\Delta p = 50\text{HPa}$ and $V_{fm} = 5.0\text{ms}^{-1}$. Solid vertical lines show mean wind direction and dashed vertical lines the peak wave direction. All angles measured anti-clockwise from x axis.

950

951

Accepted for publication in *Journal of Physical Oceanography*. DOI 10.1175/JPO-D-21-0005.1.

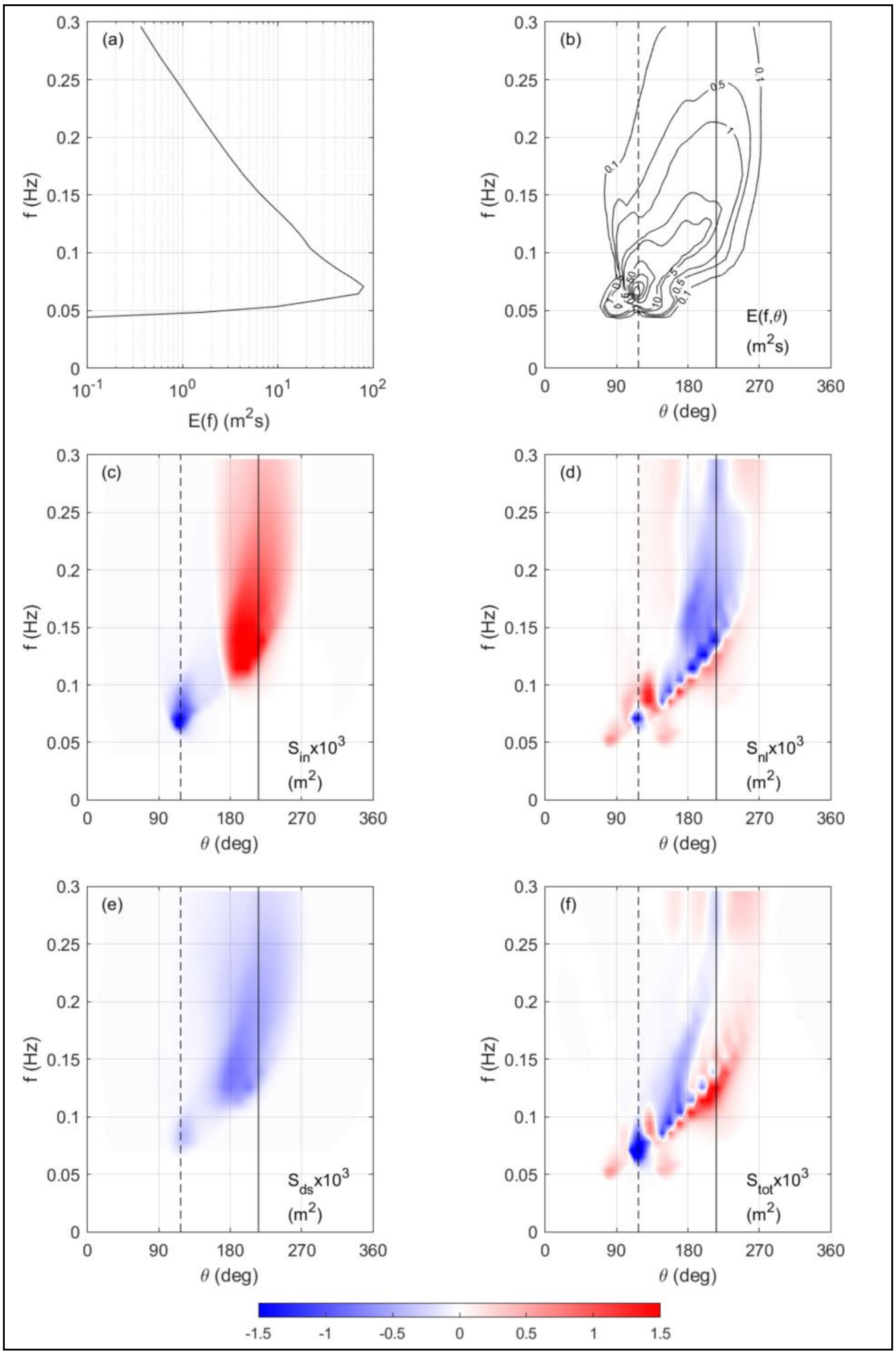

991

Figure 8. WW3 model directional spectra and source terms from a location in the NNW octant of a tropical cyclone with $\Delta p = 50$HPa and $V_{fm} = 5.0$ms^{-1}. (a) One dimensional spectrum, $E(f)$ (m^{2}s), (b) Directional spectrum, $E(f,\theta)$ (m^{2}s), contours drawn at [0.1, 0.5, 1, 5, 10, 50, 100, 200], (c) Wind input source term, $S_{in}(f,\theta)$ x10^3 (m^2), (d) Nonlinear source term, $S_{nl}(f,\theta)$ x10^3 (m^2), (e) Dissipation source term, $S_{ds}(f,\theta)$ x10^3 (m^2), (f) Total source term, $S_{tot}(f,\theta)$ x10^3 (m^2). For each panel, the vertical solid line shows the wind direction and the dashed line the peak wave direction. All angles measured anti-clockwise from x axis.

Accepted for publication in *Journal of Physical Oceanography*. DOI 10.1175/JPO-D-21-0005.1.

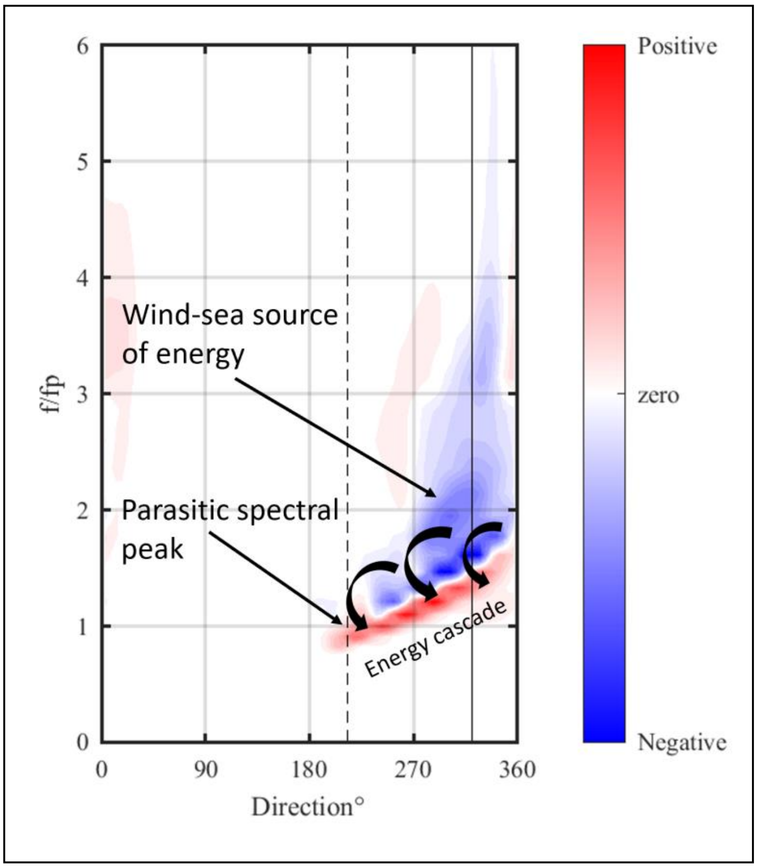

Figure 9. An example of the role played by the nonlinear term, S_{nl} in tropical cyclone wave evolution. The nonlinear term transfers energy form the wind-sea to remotely generated waves at the spectral peak. This occurs through an energy cascade along the "ridge" connecting these wave systems. As a result, the waves at the spectral peak act in a "parasitic" manner to take energy for the local wind-sea to enhance growth at the spectral peak. The process ensures that the two wave systems remain connected through the directionally skewed spectrum. The case shown is for the spectrum in the west-south-west octant of Figure 4.

Accepted for publication in *Journal of Physical Oceanography*. DOI 10.1175/JPO-D-21-0005.1.